buildings

MDPI

Article

Experimental Study on the Bending Mechanical Properties of Socket-Type Concrete Pipe Joints

Xu Liang [1], Jian Xu [1], Xuesong Song [2], Zhongyao Ren [2] and Li Shi [3,*]

[1] Hangzhou Urban Infrastructure Construction Management Center, Hangzhou Urban Rural Development Commission, Hangzhou 310006, China; lxu62103@gmail.com (X.L.); xjian6411@gmail.com (J.X.)
[2] Power China Hua Dong Engineering Co., Ltd., Hangzhou 310014, China; song_xs@hdec.com (X.S.); ren_zy@hdec.com (Z.R.)
[3] School of Civil Engineering, Zhejiang University of Technology, Hangzhou 310023, China
* Correspondence: lishi@zjut.edu.cn

Abstract: In modern infrastructure construction, the socket joint of concrete pipelines is a critical component in ensuring the overall stability and safety of the pipeline system. This study conducted monotonic and cyclic bending loading tests on DN300 concrete pipeline socket joints to thoroughly analyse their bending mechanical properties. The experimental results indicated that during monotonic loading, the relationship between the joint angle and bending moment exhibited nonlinear growth, with the stress state of the socket joint transitioning from the initial contact between the rubber ring and the socket to the eventual contact between the spigot and socket concrete. During the cyclic loading phase, the accumulated joint angle, secant stiffness, and bending stiffness of the pipeline interface significantly increased within the first 1 to 7 cycles and stabilised between the 8th and 40th cycles. After 40 cycles of loading, the bending stiffness of the joint reached 1.5 kN·m^2, while the stiffness of the pipeline was approximately 8500 times that of the joint. Additionally, a finite element model for the monotonic loading of the concrete pipeline socket joint was established, and the simulation results showed good agreement with the experimental data, providing a reliable basis for further simulation and analysis of the joint's mechanical performance under higher loads. This study fills the gap in research on the mechanical properties of concrete pipeline socket joints, particularly under bending loads, and offers valuable references for related engineering applications.

Keywords: concrete pipelines; socket joints; mechanical properties; stiffness; numerical simulation

check for updates

Citation: Liang, X.; Xu, J.; Song, X.; Ren, Z.; Shi, L. Experimental Study on the Bending Mechanical Properties of Socket-Type Concrete Pipe Joints. *Buildings* **2024**, *14*, 3655. https://doi.org/10.3390/buildings14113655

Academic Editor: Mizan Ahmed

Received: 15 October 2024
Revised: 13 November 2024
Accepted: 14 November 2024
Published: 17 November 2024

Copyright: © 2024 by the authors. Licensee MDPI, Basel, Switzerland. This article is an open access article distributed under the terms and conditions of the Creative Commons Attribution (CC BY) license (https://creativecommons.org/licenses/by/4.0/).

1. Introduction

Buried pipelines are widely used to transport vital resources, such as water, gas, and oil, for urban operations. Moreover, these pipelines are crucial components of urban lifeline projects. Concrete pipelines are commonly used owing to their simple manufacturing process and high stiffness. These pipelines often utilise a socket connection method, with a rubber ring fitted around the spigot and inserted into the socket of another pipe segment. However, past earthquake damage has shown that buried pipelines can sustain significant damage [1–4], which severely affects the post-earthquake recovery of urban functions. Earthquakes mainly induce cyclic displacements in the soil, which generate cyclic forces, such as shear, axial, and bending forces, in pipelines. Among these pipelines, the joints are the weakest parts. Consequently, most failures in concrete pipelines occur at the socket joints.

Regarding the mechanical performance of pipelines under cyclic loading, Liu et al. [5] investigated the fatigue performance and failure mechanisms of DN200 ductile iron pipelines under monotonic and two types of cyclic traffic loads through experimental and theoretical analyses. Xu et al. [6] studied the bending mechanical properties and deformation characteristics of rectangular tunnelling pipes with F-type socket joints under different upper-load conditions. Zhang et al. [7] conducted field experiments to examine

the mechanical responses of X65 pipelines under traffic loads under empty, half-loaded, and fully loaded conditions. Zhong et al. [8] simulated axial cyclic load tests on both empty and water-filled pipes to explore the performance of ductile iron push-on joints rehabilitated with CIPP liners under repeated and seismic loading conditions. O'Rourke et al. [9,10] modelled the complex interaction between the pipe and the soil as a spring–slider system and represented the pipeline joint as a nonlinear spring element. Additionally, numerical simulations were conducted to analyse the axial deformation of the pipeline joint under seismic cyclic loading. Elhmadi and O'Rourke [11] classified the pipeline into beam elements for their analysis and modelled the joints between these segments as nonlinear springs, which accounted for both axial tensile forces and lateral bending forces. The dynamic response of the buried pipeline to seismic wave input was analysed. Hosseini and Ajideh [12] modified the pipeline joint to axial and lateral elastic springs and used spring–damper elements to simulate the interaction between the pipe and the soil. Moreover, the effect of the soil stiffness on the nonlinear seismic responses of buried pipelines was investigated. Similarly, Shi [13] classified the pipeline into beam elements and incorporated the elastoplastic properties of the joint into the analysis. This approach was used to investigate and estimate the pipeline strain and the relative displacement of the joints. These studies mainly involved theoretical analyses and numerical simulations using suitable simplifications of the pipeline body and its joints.

To accurately elucidate the mechanical performance of socket-type pipelines, researchers have performed model loading tests on these pipelines. Chen Chungang et al. [14] conducted prototype pull-out tests to evaluate the pulling force and deformation of socket-type cast-iron pipeline joints. The tests confirmed that socket joints with rubber rings exhibited strong seismic performances. Considering the working conditions of pressurised and non-pressurised water in the pipes, Han et al. [15] conducted axial monotonic tensile tests on socket-type ductile iron pipelines and analysed the relationship between the joint tensile displacement and pipeline diameter. Zhong et al. [16–19] investigated the seismic performance of in situ repaired ductile iron pipelines. Vazouras and Karamanos [20] conducted both experimental and numerical simulations to investigate the mechanical properties of pipeline bends and found that these bends can effectively reduce joint displacements caused by fault movements. Rabi [21] used artificial neural networks to predict the ultimate buckling resistance of CHS (circular hollow section) beam–columns and established a finite element model for verification and parameter studies. The performance of stainless-steel-reinforced concrete beams was analysed, and a finite element model was developed to parametrise the most significant characteristics of the beams. This approach provided a reliable solution for predicting the load-bearing capacity of concrete beams reinforced with stainless steel [22,23]. Cao Jianguo [24] conducted pull-out and bending tests on flexible joints for underground water supply pipelines of two diameters and three types of materials. The results revealed that the axial load-bearing capacity of ductile iron pipelines was mainly influenced by the insertion depth.

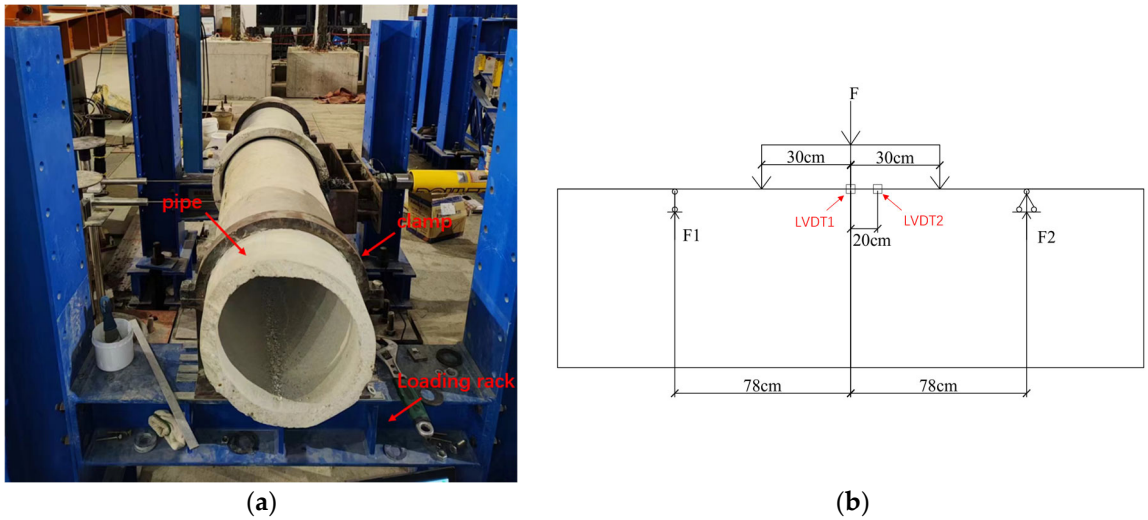
Existing research has primarily focused on the mechanical properties of ductile iron pipe joints, with relatively fewer experimental studies on concrete socket-type pipeline joints. Moreover, most existing studies concentrate on the axial mechanical performance of these joints, with less attention given to their bending performance. However, pipelines are subjected to a combination of axial, shear, and bending loads due to cyclic dynamic actions, such as seismic forces, traffic loads, and nearby shield tunnelling operations. Among these, bending loads have a direct impact on the opening deformation and failure of the joints. Therefore, a detailed investigation of the mechanical performance of concrete socket-type pipeline joints under cyclic bending loads is crucial for filling the knowledge gap in this field. Such research is of significant theoretical and practical importance for ensuring the safety of pipeline systems.

In this study, a test device was designed to apply transverse bending loads to DN300 concrete pipelines. This device was used for full-scale tests of both monotonic and cyclic bending loads on socket-type joints. The mechanical properties of the socket-type concrete

pipeline joints, such as the rotation angle and stiffness, were analysed. Additionally, a detailed finite element model (FEM) of the socket-type concrete pipeline joint was developed using ABAQUS software version 2021. Based on the comparison and verification of the model's test results, the mechanical properties of the joint under higher loads were further simulated and analysed.

2. Test Overview

In practical engineering, a trench in the foundation soil is first excavated. The pipe sections are lowered into the trench and connected to the socket joints. The trench is then backfilled to complete the installation of the socket-type pipeline. If actual construction conditions are simulated through the placement of the pipe sections in the soil or on the surface before bending loads are applied, the friction from the soil may interfere with the accurate measurement of the bending moment on the socket joint. Consequently, determining the bending stiffness of the socket joint is challenging. To address this issue, a loading frame was designed (Figure 1) with two pipe sections suspended separately. A two-point method was used to apply lateral horizontal thrust to both sides of the pipeline joint, generating a uniformly distributed bending moment between the two loading points. The horizontal thrust was applied to the pipeline joint using a jack connected to a load plate, which ensured even distribution of the load between the two points. Owing to the high stiffness of the concrete pipe body, clamps were fixed at the ends of the two pipe sections to prevent rigid body displacement during horizontal loading (Figure 1a).



(**a**) (**b**)

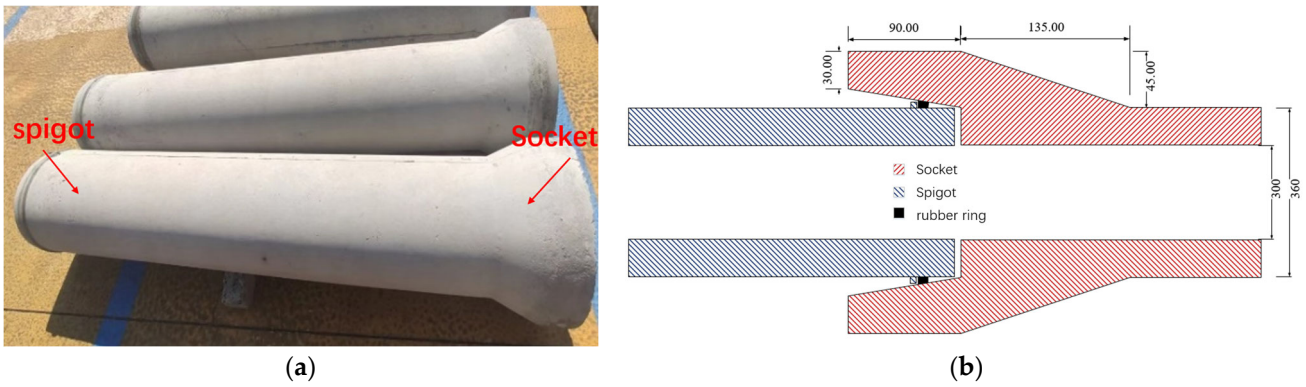
Figure 1. Flexural loading test of full-sized concrete pipeline–socket interface: (**a**) side view; (**b**) top view.

The two loading points were positioned symmetrically around the joint centreline, each 30 cm from the centreline. Additionally, two clamps were symmetrically arranged, each 78 cm from the centreline on both sides of the joint. One LVDT (linear variable differential transformer) was positioned at the centreline of the joint, while another LVDT was placed 20 cm from the centreline on the spigot side (Figure 1b). The horizontal thrust was recorded in real time using the jack, with a measurement range of 0–50 kN and an accuracy of 0.01 kN. Moreover, displacement sensors (LVDTs) were placed near the joint to measure the lateral displacement at the loading points in real time. The sensors had a measurement range of 0–200 mm and an accuracy of 0.2 mm.

2.1. Specimen Installation and Adjustment

Full-scale bending load tests were conducted on socket-type joints using DN300 concrete pipelines (Jiaxing Weili Construction Co., Ltd., Jiaxing, China), which are commonly

used in engineering practice (Figure 2a). In these pipelines, the expanded end of the pipe section formed the socket, while the other end formed the spigot. To assemble the socket joint, a rubber ring was fitted onto the spigot and then inserted into the socket, thereby completing the socket-type connection between the two pipe sections. The joint structure and dimensions are detailed in Figure 2b.



(**a**) (**b**)

Figure 2. (**a**) Physical drawing of test pipe fitting; (**b**) pipe interfacial dimensions (mm).

During the installation of socket-type concrete pipelines, misalignment can often cause uneven insertion forces, which may displace the rubber ring from its intended position, resulting in improper pipeline installation. To ensure successful joint installation, the following steps were implemented during the test preparation:

1. Cleaning the pipe ends: Both the rubber ring and pipe surface were thoroughly cleaned. The chamfer on the pipe spigot was checked to ensure it met the installation requirements;
2. Installing the rubber ring: After cleaning, the rubber ring was fitted onto the spigot, ensuring the ring was tightly adhered to the raised edge of the outer wall of the spigot;
3. Applying the lubricant: An appropriate amount of petroleum jelly was evenly applied to both the inner surface of the rubber ring and the outer surface of the spigot. Additionally, petroleum jelly was applied to the support points of the pipe sections on the loading frame and to the inner walls of the clamps to reduce interfacial friction;
4. Assembling the pipeline: First, the pipe section with the socket was positioned on the loading frame and secured with a clamp. The spigot pipe section with the fitted rubber ring was then lifted and inserted into the socket, thereby completing the assembly of the pipeline specimen. The assembled joint is shown in Figure 3.

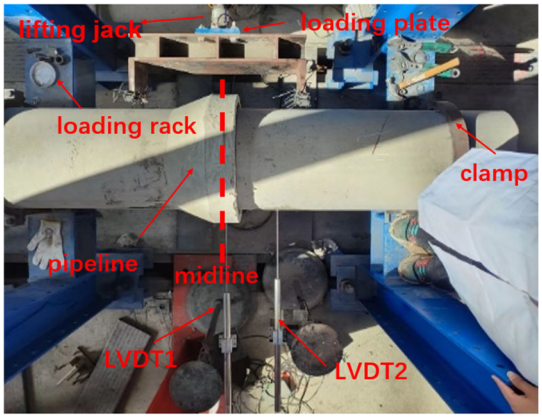


Figure 3. Assembly diagram of the pipeline–socket interface.

2.2. Calculation of Bending Moment and Rotation Angle

Because the flexural load-bearing capacity of the pipeline joint was significantly lower than that of the pipe section, the pipe body can be considered as rigid in the bending load tests. The bending moment and rotation angle at the pipeline joint were calculated using geometric relationships based on the measured results. The pipe had an outer diameter of 360 mm, while the clamps at both ends had an inner diameter of 360 mm and a thickness of 10 mm. These clamps restricted the lateral movement of the pipe at their positions but enabled low-angle rotations, making them function as hinged supports (Figure 4).

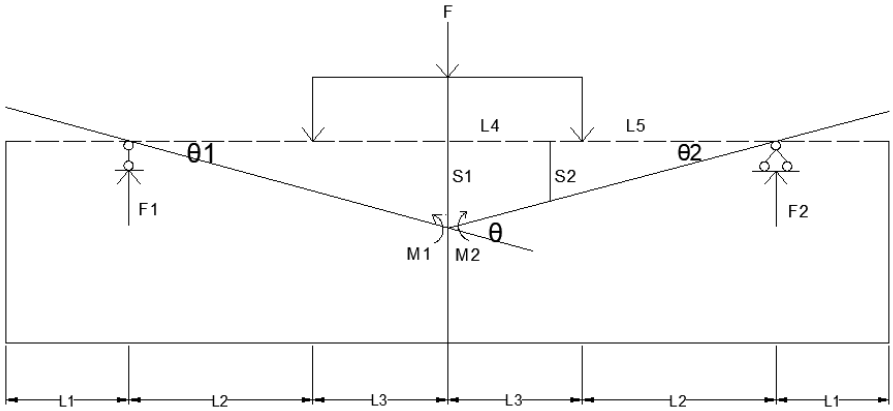


Figure 4. Calculation diagram of pipeline interfacial bending deformation.

Because the joint rotation angle could not be directly measured during the experiment, the displacement needed to be converted. The displacement measured by the displacement sensors was converted to the rotation angle of the pipeline joint based on the geometric relationship (Figure 4). Moment equilibrium equations were first established for the pipe sections on both sides of the joint (Equation (1)). The bending resistance of the pipeline joint was then calculated, and the average of these values was used to determine the bending moment at the joint.

$$M = \frac{M_1 + M_2}{2} = \frac{F_1 + F_2}{2} \times (L_2 + L_3) - \frac{F}{2} \times L_3 = \frac{L_2}{2} F \quad (1)$$

where M represents the bending moment at the pipeline joint; M_1 denotes the bending resistance at the pipeline joint, calculated using the moment equilibrium applied to the left-side pipe section, $M_1 = F_1 \times (L_2 + L_3) - \frac{F}{2} \times L_3$; M_2 indicates the bending resistance at the pipeline joint, calculated using the moment equilibrium applied to the right-side pipe section, $M_2 = F_2 \times (L_2 + L_3) - \frac{F}{2} \times L_3$; F represents the applied load, with F_1 and F_2 being the reactions at the supports, as determined by the force equilibrium of the pipeline, $F = F_1 + F_2$; S_1 and S_2 denote the displacements measured by the transducers at their corresponding positions; θ represents the rotation angle at the joint.

$$\theta = \theta_1 + \theta_2 = \arctan\frac{S_1}{L_2 + L_3} + \arctan\frac{S_2}{L_5}$$

2.3. Loading Scheme

Monotonic and cyclic bending load tests were conducted on the socket-type concrete pipeline joints. The test schemes are shown in Table 1. Test 1 employed a load control method, with a gradual increase in the load at a rate of 0.15 kN/s up to 30 kN. Each test specimen underwent testing in triplicate to ensure the reliability and accuracy of the results. Tests 2 and 3 involved cyclic loading tests, with load values selected from Stages 2 and 3 of the monotonic loading used as cyclic load amplitudes of 10.5 and 17.5 kN. The cyclic loading and unloading rates were both set at 0.15 kN/s, and each cycle was repeated 40 times. Figure 5 shows the time-history curves of the jack's cyclic load for Tests 2 and 3.

Table 1. Test protocol.

Test Number	Loading Rate (kN/s)	Loading Method	Load Value (kN)
test 1	0.15	monotonic loading	0–30
test 2	0.15	cyclic loading	0–10.5
test 3	0.15	cyclic loading	0–17.5

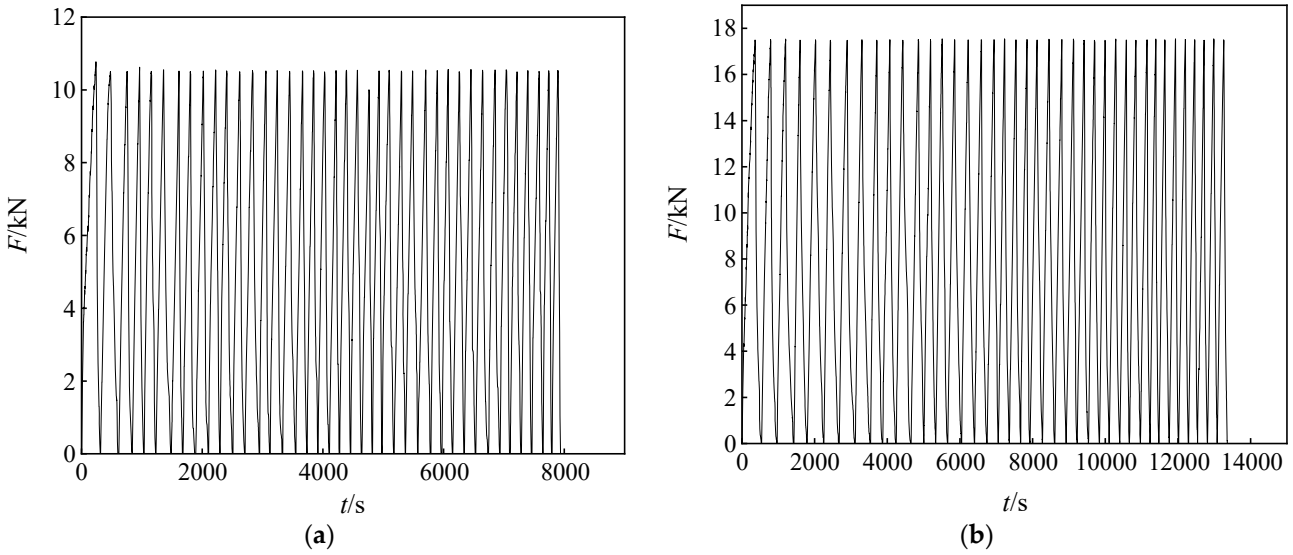


Figure 5. Cyclic loading time-history curves: (**a**) Test 2 with a cyclic load amplitude of 10.5 kN; (**b**) Test 3 with a cyclic load amplitude of 17.5 kN.

3. Test Results and Analysis

3.1. Mechanical Properties of Socket Joints Under Monotonic Loading

Figure 6 shows typical images from the monotonic loading test. The rubber ring created a 1–2 mm gap between the outer wall of the spigot and the inner wall of the socket in the assembled pipeline. During monotonic loading, the pipeline joint exhibited significant lateral displacement (Figure 6b), which progressively increased with increasing applied load. Over time, contact between the socket and spigot gradually developed.

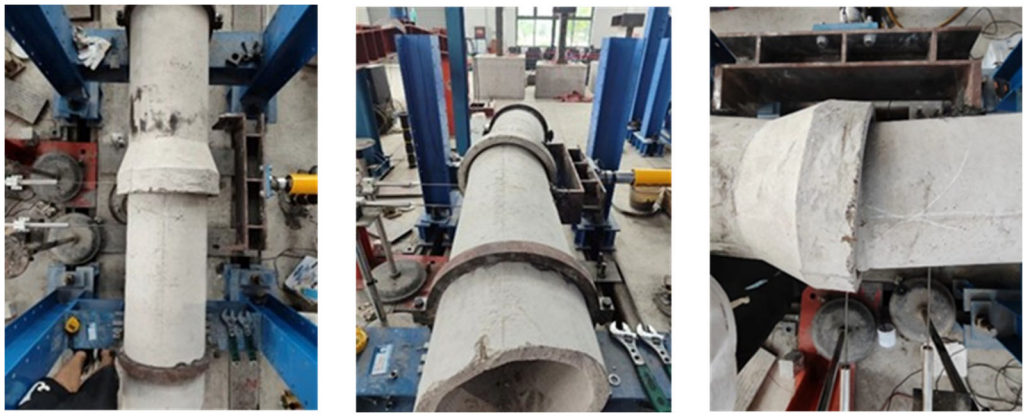


Figure 6. Monotonic bending loading test process for pipeline joints: (**a**) before loading; (**b**) during loading; (**c**) after loading.

Figure 7 presents the load–displacement curves of the socket joint from three monotonic loading tests. Under lateral loading, the socket joint undergoes three deformation

stages. In Stage 1, the load on the pipeline joint rapidly increases with increasing displacement, indicating a nonlinear relationship. At this stage, the socket joint reaches a maximum lateral displacement of 2.9 mm with a lateral load of 6.2 kN owing to the tolerance matching of various components. In Stage 2, the load on the pipeline joint continuously increases with increasing displacement, indicating a nearly linear relationship between the load and the displacement. During this stage, the load-bearing capacity of the joint mainly depends on the compression of the rubber ring and the friction between the rubber ring and both the inner wall of the socket and the outer wall of the spigot. As the lateral displacement of the joint exceeds 19.3 mm, Stage 3 is reached. In Stage 3, the slopes of the curves in Stage 3 of the three tests are 0.67, 0.61, and 0.69, which are significantly steeper than the corresponding slopes observed in Stage 2 (0.42, 0.38, and 0.40). At this stage, direct 'hard contact' between the socket and spigot is observed, leading to a significant increase in the bending stiffness of the joint.

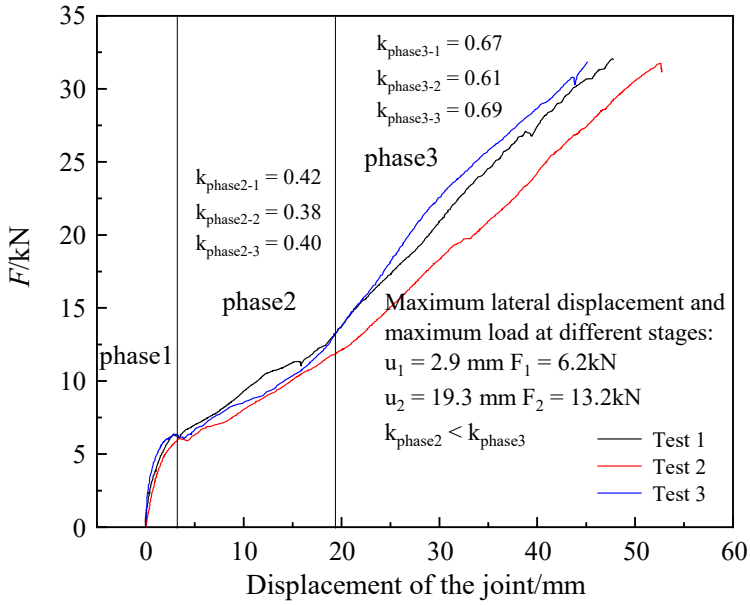


Figure 7. Load (jack's output)–displacement curves of the concrete pipeline–socket interface under monotonic loading.

During Stage 3, the rubber ring undergoes twisting deformation and sliding, leading to 'hard contact' between the socket and spigot (Figure 8). Even after the load is removed, the sliding and twisting deformations of the rubber ring remain irreversible.

According to the method depicted in Figure 4, the force applied by the jack and the displacement measured by the LVDT are converted to the bending moment and rotation angle of the socket joint. The bending moment–rotation angle curves are plotted (Figure 9). At a rotation angle of 0.5°, the joint bending deformation transitions to Stage 2. As the joint rotation angle approaches 2.8°, the slopes of the three test curves significantly increase from 0.65, 0.59, and 0.63 to 1.01, 0.96, and 1.07, respectively. This marked increase in the slope indicates a transition to Stage 3, characterised by "hard contact" between the inner wall of the socket and the outer wall of the spigot, which increases the risk of joint failure. Before reaching 2.8°, the joint undergoes flexural rotational deformation owing to the compression of the rubber ring, indicating a relatively safe normal operating stage.

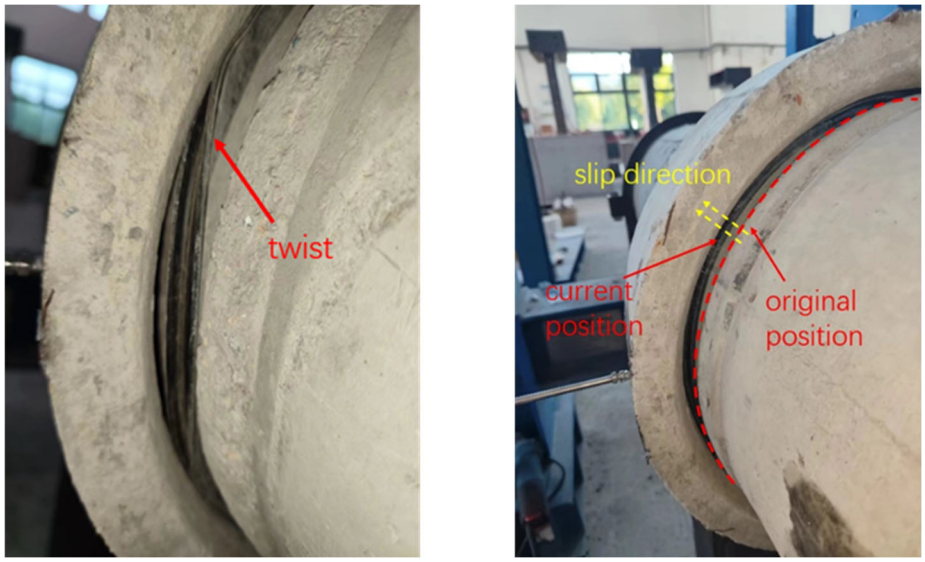


Figure 8. Rubber ring deformation during bending loading of concrete pipeline socket joints: (**a**) twist; (**b**) slippage.

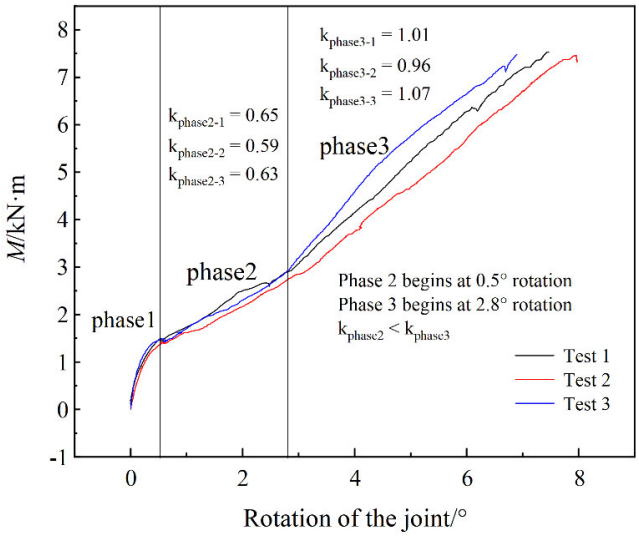


Figure 9. Moment–rotation angle curves of concrete pipeline–socket interface under monotonic loading.

3.2. Mechanical Properties of Socket Joints Under Cyclic Loading

The monotonic loading test results reveal that Stages 2 and 3 represent the normal service state and the failure-prone state of the socket-type concrete pipeline joint, respectively. Therefore, representative loads from Stages 2 and 3 (10.5 kN and 17.5 kN) are selected as the peak loads for cyclic loading tests on the joint.

3.2.1. Cumulative Rotation Angle of Pipeline Joints

Figure 10 shows the trends in the cumulative rotation angle of the pipeline joint with increasing number of cycles for two peak loads (Tests 2 and 3). As the number of cycles increases, the deformation of the pipeline joint accumulates, but the rate of the increase gradually decreases. The cumulative rotation angle as a function of the number of cycles can be categorised into three stages. In Segment OA (the first cycle), the cumulative rotation angle increases rapidly, accounting for 57.4% (Test 2) and 74.8% (Test 3) of the total cumulative rotation. In Segment AB (Cycles 2–7), the rate of the rotation angle decreases, but the overall increase remains significant, representing 28% and 19.5% of the

total cumulative rotation for Tests 2 and 3, respectively. In Segment BC (Cycles 8–40), the rotation angle slowly increases, accounting for 14.6% and 5.7% of the total cumulative rotation in Tests 2 and 3, respectively. During the first cycle, most of the rotation angle accumulates mainly owing to the compression of the rubber ring under the initial load, which causes significant deformation at the joint (Figure 11). After the load is removed, the joint rotation angle rebounds only slightly owing to friction between the rubber ring, socket, and spigot.

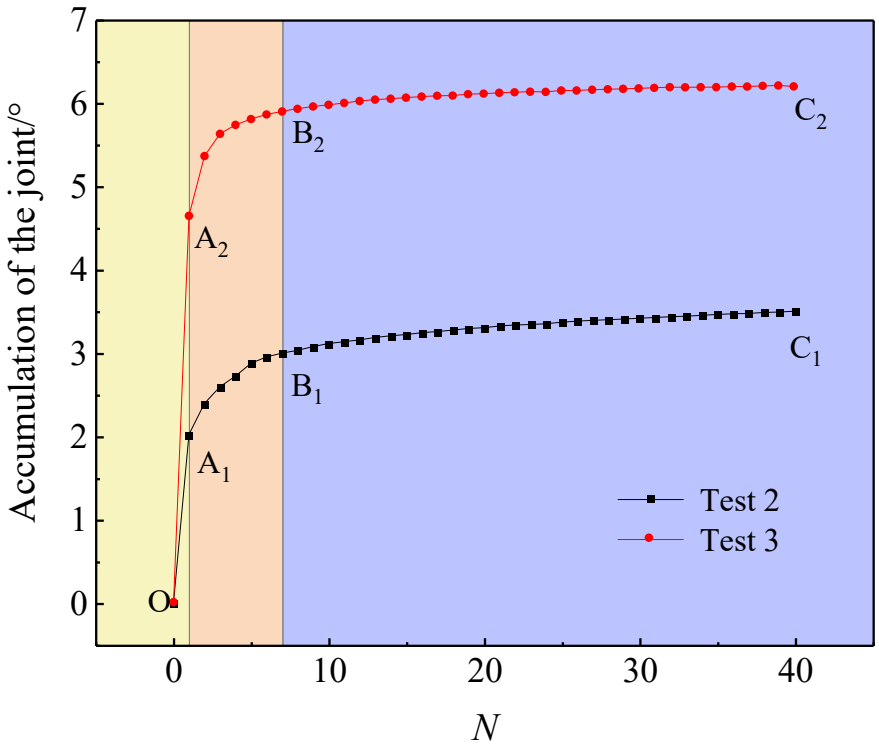


Figure 10. Cumulative rotation angles and numbers of cycles for the concrete pipeline–socket interface under cyclic loading. Note: The letters (O, A, B, C) in the figure are used to differentiate the segments of the curve.



Figure 11. Deformation of the concrete pipeline–socket interface under cyclic loading.

3.2.2. Hysteresis Loop of Joint Bending Moment–Rotation Angle

Figure 12 presents the curves illustrating the relationship between the bending moment and rotation angle of the socket-type concrete pipeline joint under cyclic loading. Generally, the loading phase of the first cycle exhibits a behaviour similar to that observed in the monotonic loading test. In the unloading phase of the first cycle, the lateral displacement (or rotation angle) of the socket joint does not fully recover, indicating minimal elastic rebound. This suggests that the joint undergoes significant irreversible plastic deformation.

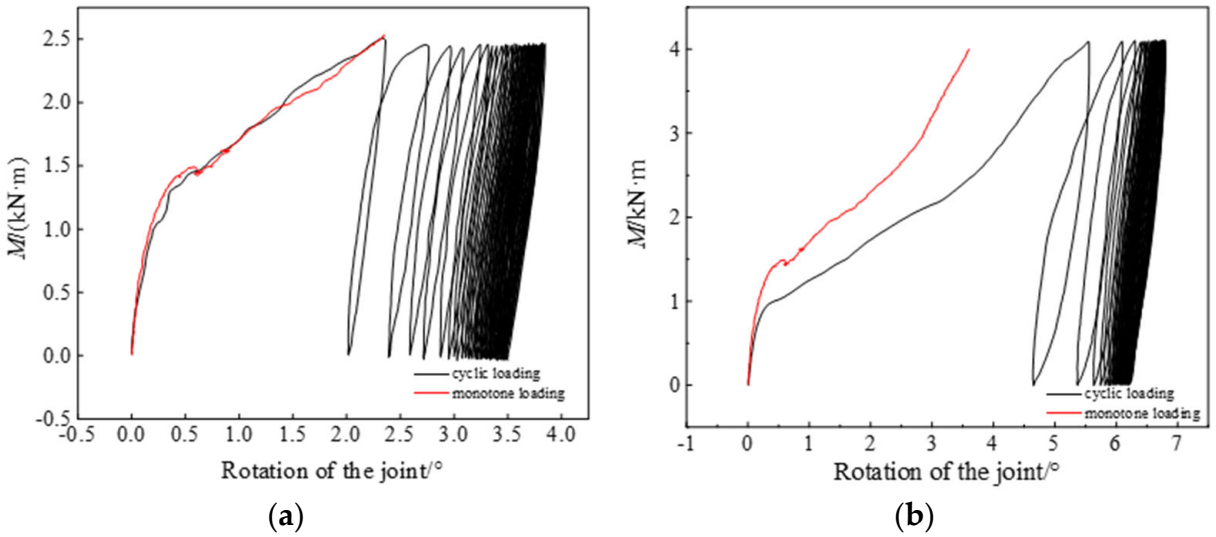


Figure 12. Bending moment–rotation angle curves for cyclic loading tests on the concrete pipeline–socket interface: (**a**) Test 2 (peak cyclic load of 10.5 kN); (**b**) Test 3 (peak cyclic load of 17.5 kN).

Moreover, cyclic loading and unloading form a distinct hysteresis loop. As the number of cycles increases, this loop gradually shifts to the right, indicating significant deformation accumulation at the joint. Additionally, with increasing number of loading cycles, the hysteresis loop transitions from an open to a closed shape, and the area of the loop gradually decreases over time. This suggests that as the number of loading cycles increases, the growth rate of the joint rotation angle decreases. In the later stages of cycling, individual loading cycles contribute almost no additional cumulative rotation, indicating that the joint behaviour approaches a linear elastic state.

To quantitatively analyse changes in stiffness, the secant stiffness (k) of the pipeline joint is defined as the ratio of the load increment to the rotation angle increment for each loading cycle (Figure 13). This is expressed by the following equation:

$$k = \frac{F_{\max} - F_{\min}}{\theta_{\max} - \theta_{\min}} \tag{2}$$

where $F_{\max} - F_{\min}$ and $\theta_{\max} - \theta_{\min}$ represent the difference in the load and the corresponding difference in the rotation angle for a single loading cycle.

Figure 14 shows the variations in the secant stiffness with increasing number of cycles. Overall, the secant stiffness increases with increasing number of cycles. During the first seven cycles, the secant stiffness significantly increases and then gradually stabilises from the 8th to the 40th cycles.

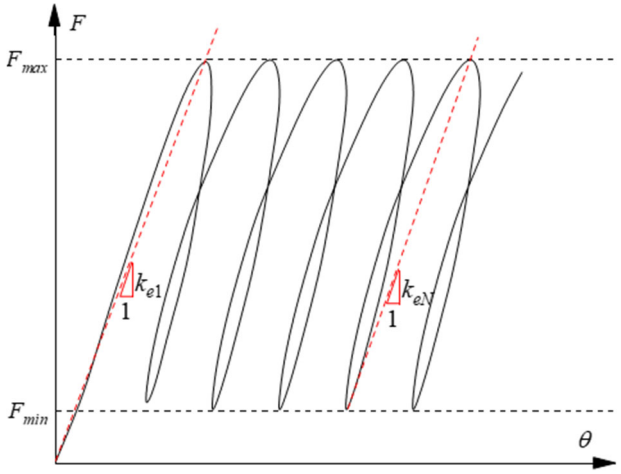


Figure 13. Secant stiffness of the cyclic hysteresis curve. Note: The black line represents the load-angle diagram in the cyclic experiment, while the red line indicates the chord of the curve.

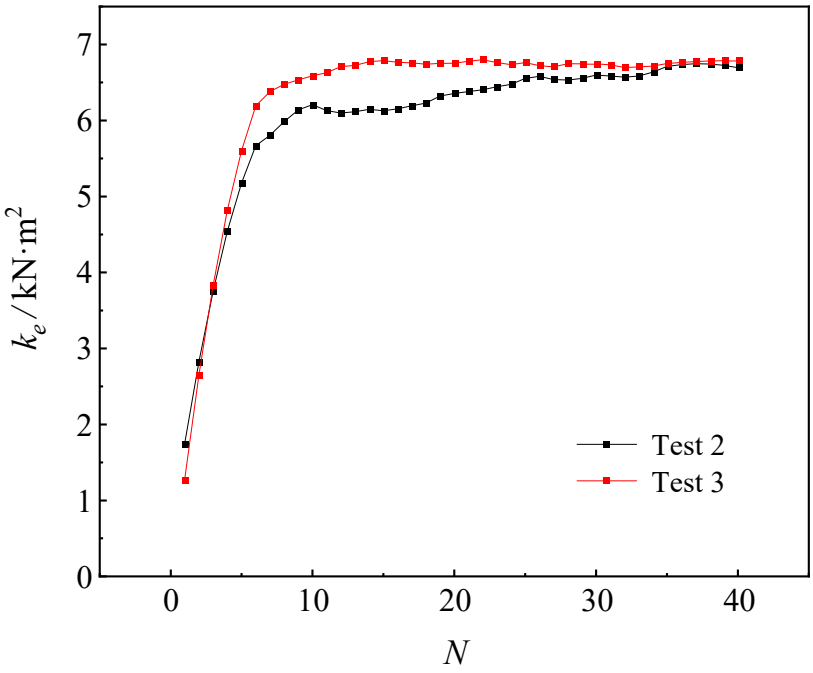


Figure 14. Variation curves of secant stiffness at the concrete pipeline–socket interface with increasing number of cycles.

3.2.3. Flexural Stiffness of the Joint

Flexural stiffness directly indicates the resistance of the pipeline to bending deformation. The flexural stiffness (k) of the socket joint is calculated using the following formula:

$$k_c = \frac{M}{\frac{d\theta}{dx}} \tag{3}$$

where M represents the bending moment at the pipeline joint, θ denotes the joint rotation angle, and x indicates the joint length.

Figure 15 shows the variations in the flexural stiffness (k_c) of the socket joint with increasing number of cycles. The flexural stiffness of the joint increases with increasing number of cycles, consistent with the trend observed in the secant stiffness (Figure 14). This increase is mainly because of the resistance of the pipeline joint to bending, which

is enhanced through the compression of the rubber ring and friction between the rubber ring and socket joint (known as 'soft contact') during the early stages of cyclic loading. As cyclic loading progresses, the resistance to bending gradually shifts to the friction between the concrete surfaces of the socket and spigot (known as 'hard contact'). Additionally, the stiffening of the rubber material leads to higher joint stiffness during the middle phase of cyclic loading (Cycles 8–30) in Test 3 (with a peak load of 17.5 kN) compared with Test 2 (with a peak load of 10.5 kN). However, in the later stages of cyclic loading (Cycles 35–40), the 'hard contact' between the concrete surfaces of the socket and spigot causes the flexural stiffness of the joint in Tests 2 and 3 to converge. Notably, within the load range of the cyclic tests conducted in this study, no crushing or other damage to the concrete of the socket joint is observed.

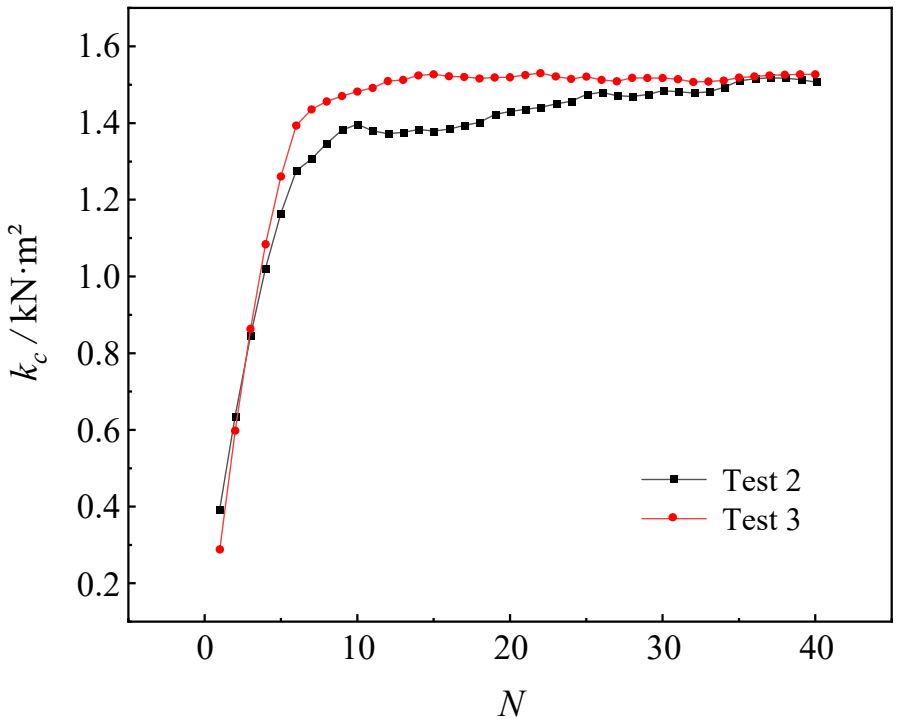


Figure 15. Curves of flexural stiffness of concrete pipeline–socket interface with increasing number of cycles.

After cycling, the socket joint exhibits a stabilised flexural stiffness (k_c) of 1.5 kN·m^2, which is 0.012% of the flexural stiffness (k_g) of the concrete pipe body (C30 concrete) at 12,800 kN·m^2 (Figure 15).

4. Numerical Simulations

4.1. Introduction to the Three-Dimensional (3D) Numerical Model

The FEM of the socket-type concrete pipeline was developed using ABAQUS finite element analysis software version 2021 (Figure 16). The dimensions of the socket and spigot are detailed in Figure 2, and each pipe section, including the socket and spigot, was modelled as 1 metre long in the FEM. The pipeline material in the model had an elastic modulus of 30 GPa (corresponding to C30 concrete), a Poisson's ratio of 0.3, and a mass density of 2300 kg/m^3. The rubber ring had an elastic modulus of 2 MPa, a Poisson's ratio of 0.45, and a density of 1200 kg/m^3 (Xu et al. [25]). The boundary condition is specified as fully fixed at both ends of the pipeline. Both the pipeline and the rubber ring were modelled using C3D8R elements.

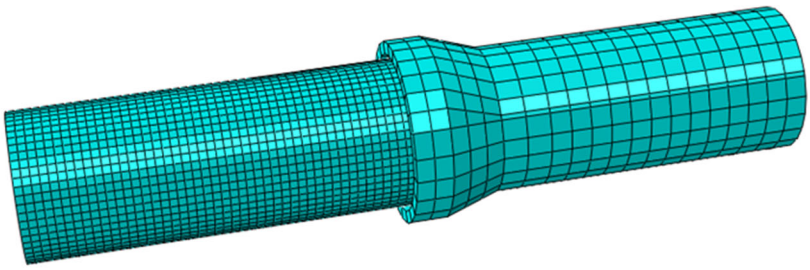


Figure 16. Three-dimensional finite model grid diagram of the concrete pipeline–socket interface.

Considering the potential slip between the rubber ring and socket joint, contact elements were defined between the outer wall of the spigot and the rubber ring and between the inner wall of the socket and the rubber ring. In the tangential direction, a 'penalty' function with a friction coefficient of 0.3 was applied, while the normal direction perpendicular to the contact surfaces utilised 'hard contact'. Similar to the monotonic loading test, a two-point method was used to apply a monotonic bending moment load to the joint, with both ends of the pipeline fully fixed.

4.2. Comparison of Results

Stage 1 of the test curve can be attributed to the tolerance matching of the test instruments, which is not required in numerical simulations. Therefore, the finite element simulation results were compared with the test results for Stages 2 and 3 (Figure 17).

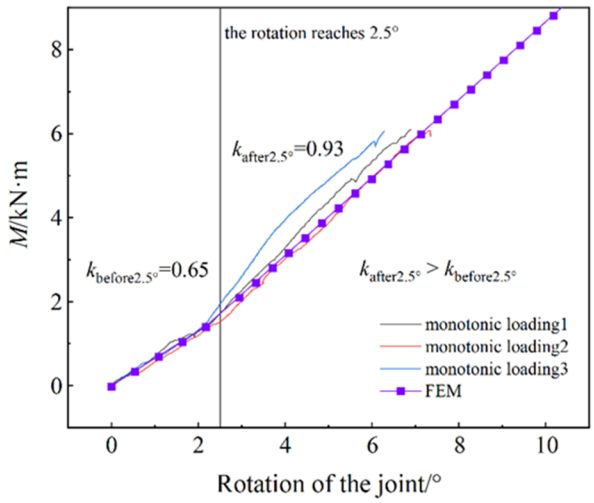


Figure 17. Bending moment–rotation angle curves of the concrete pipeline–socket interface under monotonic loading and corresponding numerical simulation.

The bending moment–rotation angle curve obtained from the numerical simulation was nearly consistent with the test results (Figure 17). The bending moment of the pipeline joint increased with increasing rotation angle. Moreover, a relationship was observed between the bending moment and the rotation angle. The load-bearing capacity of the joint mainly depended on the compression of the rubber ring and the friction between the rubber ring and both the inner wall of the socket and the outer wall of the spigot. As the joint rotation angle exceeded 2.5°, the slope of the curve significantly steepened from 0.65 to 0.93, indicating 'hard contact' between the socket and spigot, which limited further joint deformation. To gain a clearer understanding of the model's convergence behaviour and to validate the accuracy of the numerical simulation, the effects of different mesh quantities on the maximum displacement of the joint under a bending moment of 8 kN·m were analysed as shown in Table 2.

Table 2. The effect of different mesh quantities on the maximum displacement.

Test Number	Mesh Number	U, Magnitude (mm)
1	4000	79.1
2	6000	81.2
3	8000	82.3

As the bending moment on the joint exceeded 7.5 kN·m, the loading frame might undergo overall displacement, which would prevent further loading owing to the limited loading capacity of the test apparatus. However, the numerical model developed in this study predicted the trend of the bending moment–rotation angle curve for the socket-type concrete pipeline joint as the load continuously increased (Figure 18).

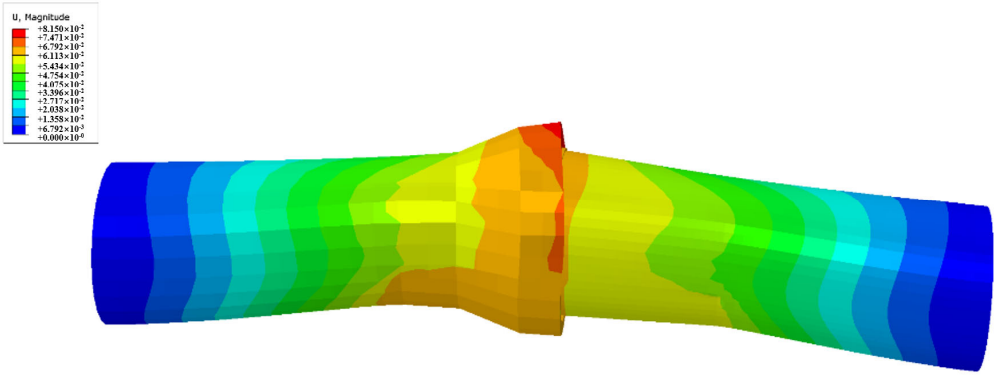


Figure 18. Displacement cloud map of the concrete pipeline–socket interface under a bending moment of 8 kN·m.

The bending moment–rotation angle data up to 12° can be obtained through finite element simulations. As the joint rotation angle reached 12°, the socket and spigot were nearly fully separated, which could result in leakage of the pipeline medium (e.g., water) and lead to pipeline failure.

For example, Figures 18 and 19 show the displacement and stress distribution cloud maps of the joint under a bending moment of 8 kN·m.

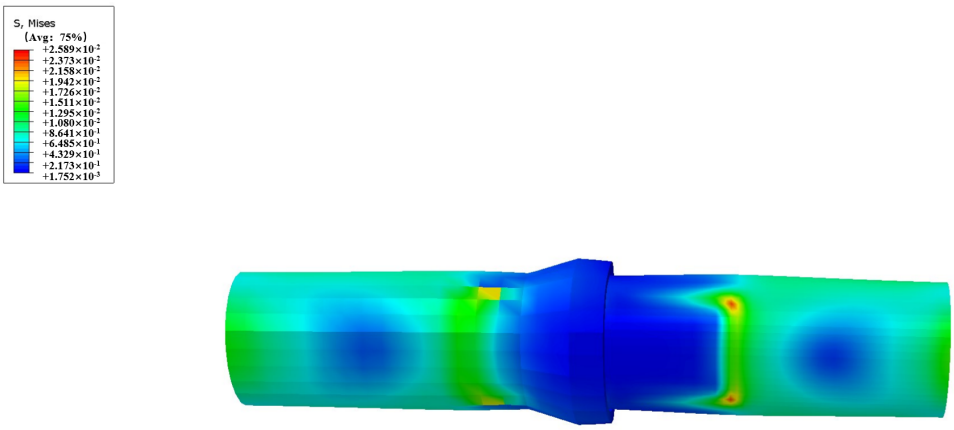


Figure 19. Stress distribution cloud map of the concrete pipeline–socket interface under a bending moment of 8 kN·m.

5. Conclusions

A 'two-point method' lateral loading test device was designed to quantitatively assess the bending performance of socket-type concrete pipeline joints. The bending mo-

ment and rotation angle of the joint were determined using force balance and geometric deformation relationships.

Monotonic and cyclic loading tests were conducted on DN300 concrete pipeline socket joints, and the relationship between the bending moment and rotation angle was determined. The secant stiffness and flexural stiffness of the joint were calculated.

Moreover, a 3D FEM of the concrete socket joint was developed, and a simulated bending moment loading was applied. Through the comparison of these results with those from the monotonic loading test, the deformation characteristics of the joint at high rotation angles were analysed.

The main conclusions are as follows:

1. The bending moment–rotation angle curve of the socket joint undergoes three stages. In Stage 1, the load on the pipeline joint increases with increasing displacement, indicating a nonlinear relationship between the load and the displacement. During this stage, the lateral displacement is limited to a maximum of 2.9 mm owing to the tolerance matching of various components. In Stage 2, the load on the pipeline joint increases with increasing displacement, indicating a linear relationship between the load and the displacement. At this stage, the load-bearing capacity of the joint mainly depends on the compression of the rubber ring and the friction between the rubber ring and both the inner wall of the socket and the outer wall of the spigot. In Stage 3, the slope of the curve at this stage is significantly steeper than that in Stage 2, indicating 'hard contact' between the socket and spigot, which significantly increases the flexural stiffness of the joint;
2. During the cyclic loading tests, most of the rotation angle of the joint accumulates in the first cycle. As the number of cycles increases, the deformation of the pipeline joint continuously accumulates, but the rate of the increase gradually decreases over time. In the later stages of cycling, the additional accumulation of the rotation angle is minimal, indicating that the joint behaviour approaches a linear elastic state. Under cyclic loading, the socket-type concrete joint exhibits a stabilised flexural stiffness of 1.5 kN·m^2, which is only 0.012% of the flexural stiffness of the concrete pipe section (C30 concrete, 12,800 kN·m^2);
3. During the first 1–7 cycles, both the secant stiffness and flexural stiffness of the socket-type concrete joint significantly increase. From the 8th to the 40th cycles, the rate of the increase in the stiffness slows down. In the intermediate phase of cyclic loading (Cycles 8–30), the rubber material exhibits higher joint stiffness under higher peak load conditions (17.5 kN, Test 2) compared with lower peak load conditions (10.5 kN, Test 2). This increase may be attributed to the stiffening effect of the material. However, in the later stages of cyclic loading (Cycles 35–40), 'hard contact' between the concrete surfaces of the socket and spigot causes the flexural stiffness of the joint to converge, regardless of the load conditions.

Author Contributions: Conceptualisation, X.L. and Z.R.; methodology, X.L. and J.X.; software, X.S.; formal analysis, J.X. and Z.R.; investigation, J.X. and X.S.; resources, X.L. and L.S.; data curation, J.X.; writing—original draft preparation, J.X., X.S. and Z.R.; writing—review and editing, X.L. and L.S.; visualisation, Z.R.; supervision, X.L. and L.S. All authors have read and agreed to the published version of the manuscript.

Funding: This research was funded by Zhejiang Province Construction Research Projects (2023K155).

Data Availability Statement: The data are available upon reasonable request.

Conflicts of Interest: Authors Xuesong Song and Zhongyao Ren were employed by the company Power China Hua Dong Engineering Co., Ltd. The remaining authors declare that the research was conducted in the absence of any commercial or financial relationships that could be construed as a potential conflict of interest.

References

1. Scawthorn, C.; O'Rourke, T.D.; Blackburn, F.T. The 1906 San Francisco Earthquake and Fire—Enduring Lessons for Fire Protection and Water Supply. *Earthq. Spectra* **2006**, *22*, 135–158. [CrossRef]
2. O'Rourke, T.D.; Bonneau, A.L.; Pease, J.W.; Shi, P.; Wang, Y. Liquefaction and Ground Failures in San Francisco. *Earthq. Spectra* **2006**, *22*, 91–112. [CrossRef]
3. Ayala, A.G.; O'Rourke, M.J.; Escobar, J.A. Evaluation of the Effects of the 1985 Michoacan Earthquake on the Water Systems in Metropolitan Mexico City. *Earthq. Spectra* **1990**, *6*, 473–496. [CrossRef]
4. Shu, Y. Comprehensive analysis of seismic damage and key issues in the seismic capacity of existing water supply and drainage pipelines. *Urban Roads Bridges Flood Control* **2013**, *3*, 111–114+216–217. (In Chinese)
5. Liu, W.; Cui, W. Fatigue Performance and Failure Mechanism of Ductile Iron Pipes with Socket Joints under Traffic Loads. *Eng. Fail. Anal.* **2024**, *167*, 109004. [CrossRef]
6. Xu, Y.; Huang, Z.; Zhang, C.; Pang, Y.; Liu, T. Bearing Capacities and Failure Behaviors of F-Type Socket Joint in Rectangular Pipe Jacking Tunnel. *Appl. Sci.* **2023**, *13*, 5442. [CrossRef]
7. Zhang, D.; Liu, X.; Yang, Y.; Shi, N.; Jiang, J.; Chen, P.; Wu, X.; Gao, H.; Zhang, H. Field Experiment and Numerical Investigation on the Mechanical Response of Buried Pipeline under Traffic Load. *Eng. Fail. Anal.* **2022**, *142*, 106734. [CrossRef]
8. Zhong, Z.; Wang, S.; Zhao, M.; Du, X.; Li, L. Performance of Ductile Iron Push-on Joints Rehabilitated with CIPP Liner under Repetitive and Seismic Loadings. *Soil Dyn. Earthq. Eng.* **2018**, *115*, 776–786. [CrossRef]
9. O'Rourke, M.J.; Liu, X. *Seismic Design of Buried and Offshore Pipelines*; MCEER: Buffalo, NY, USA, 2012.
10. O'Rourke, T.D.; Jeon, S.S.; Toprak, S.; Cubrinovski, M.; Hughes, M.; Ballegooy, S.V.; Bouziou, D. Earthquake Response of Underground Pipeline Networks in Christchurch, NZ. *Earthq. Spectra* **2014**, *30*, 183–204. [CrossRef]
11. Elhmadi, K.; O'Rourke, M.J. Seismic Damage to Segmented Buried Pipelines. *Earthq. Eng. Struct. Dyn.* **1990**, *19*, 529–539. [CrossRef]
12. Castronovo, J.P. Pipelines 2001: Advances in Pipelines Engineering and Construction. In Proceedings of the Pipeline Division Specialty Conference 2001, San Diego, CA, USA, 15 July 2001.
13. Shi, P. Seismic Wave Propagation Effects on Buried Segmented Pipelines. *Soil Dyn. Earthq. Eng.* **2015**, *72*, 89–98. [CrossRef]
14. Chen, C.; Yang, Q.; Kong, J.; Xie, X.; Liao, Q. Experimental Study on the Seismic Performance of Rubber Gasketed Bell-and-Spigot Joints in Cast Iron Pipelines. In Proceedings of the Earthquake Engineering and Engineering Vibration Conference, Lisbon, Portugal, 28 September 2012; pp. 104–108. (In Chinese)
15. Yang, H.; Hongling, S.; Lei, Z.; Junfeng, D. Experimental Research on Ductile Iron Pipes with Rubber Gasketed Joints. In Proceedings of the Pipeline Division Specialty Conference (PIPELINES 2010), Keystone, CO, USA, 28 August–1 September 2010; pp. 1170–1176.
16. Zhong, Z.; Filiatrault, A.; Aref, A. Experimental Performance Evaluation of Pipelines Rehabilitated with Cured-In-Place Pipe Liner under Earthquake Transient Ground Deformations. *J. Infrastruct. Syst.* **2016**, *23*, 04016036. [CrossRef]
17. Zhong, Z.; Filiatrault, A.; Aref, A. Seismic Performance Evaluation of Buried Pipelines Retrofit with Cured-in-Place-Pipe Lining Technology. In Proceedings of the 16th World Conference on Earthquake, 16WCEE 2017, Santiago, Chile, 9–13 January 2017.
18. Zhong, Z.; Filiatrault, A.; Aref, A. Numerical Simulation and Seismic Performance Evaluation of Buried Pipelines Rehabilitated with Cured-in-place-pipe Liner under Seismic Wave Propagation. *Earthq. Eng. Struct. Dyn.* **2017**, *46*, 811–829. [CrossRef]
19. Zhong, Z.; Bouziou, D.; Wham, B.; Filiatrault, A.; Aref, A.; O'Rourke, T.D.; Stewart, H.E. Seismic Testing of Critical Lifelines Rehabilitated with Cured in Place Pipeline Lining Technology. *J. Earthq. Eng.* **2014**, *18*, 964–985. [CrossRef]
20. Vazouras, P.; Karamanos, S.A. Structural Behavior of Buried Pipe Bends and Their Effect on Pipeline Response in Fault Crossing Areas. *Bull. Earthq. Eng.* **2017**, *15*, 4999–5024. [CrossRef]
21. Rabi, M.; Abarkan, I.; Shamass, R. Buckling Resistance of Hot-Finished CHS Beam-Columns Using FE Modelling and Machine Learning. *Steel Constr.* **2024**, *17*, 93–103. [CrossRef]
22. Rabi, M.; Cashell, K.A.; Shamass, R. Analysis of Concrete Beams Reinforced with Stainless Steel. In Proceedings of the Fib Symposium 2019: Concrete–Innovations in Materials, Design and Structures, Krakow, Poland, 27 May 2019; pp. 690–697.
23. Rabi, M.; Cashell, K.A.; Shamass, R. Flexural Analysis and Design of Stainless Steel Reinforced Concrete Beams. *Eng. Struct.* **2019**, *198*, 109432. [CrossRef]
24. Cao, J. Experimental Study on Damage to Water Supply Pipelines under Large Ground Deformation and Seismic Safety Assessment. Master's Thesis, Zhejiang University, Hangzhou, China, 2014. (In Chinese)
25. Xu, M.; Shen, D.; Rakitin, B. The Longitudinal Response of Buried Large-Diameter Reinforced Concrete Pipeline with Gasketed Bell-and-Spigot Joints Subjected to Traffic Loading. *Tunn. Undergr. Space Technol.* **2017**, *64*, 117–132. [CrossRef]

Disclaimer/Publisher's Note: The statements, opinions and data contained in all publications are solely those of the individual author(s) and contributor(s) and not of MDPI and/or the editor(s). MDPI and/or the editor(s) disclaim responsibility for any injury to people or property resulting from any ideas, methods, instructions or products referred to in the content.